Available online at www.sciencedirect.com
ScienceDirect
Surface Science 601 (2007) 1898–1908
SURFACE SCIENCE
www.elsevier.com/locate/susc

Formation and characterization of Au/Pd surface alloys on Pd(1 1 1)

Zhenjun Li, Feng Gao, Yilin Wang, Florencia Calaza, Luke Burkholder, Wilfred T. Tysoe *

Department of Chemistry and Biochemistry, and Laboratory for Surface Studies, University of Wisconsin-Milwaukee, Milwaukee, WI 53211, USA

Received 27 December 2006; accepted for publication 26 February 2007
Available online 1 March 2007

Abstract

The formation of alloys by adsorbing gold on a Pd(1 1 1) single crystal substrate and subsequently annealing to various temperatures is studied in an ultrahigh vacuum by means of Auger and X-ray photoelectron spectroscopy. The nature of the alloy surface is probed by CO chemisorption using temperature-programmed desorption and reflection-absorption infrared spectroscopy. It is found that gold grows in a layer-by-layer fashion on Pd(1 1 1) at 300 K, and starts to diffuse into the bulk after annealing to above ~600 K. Alloy formation results in a ~0.5 eV binding energy decrease of the Au 4f XPS signals and a binding energy increase of the Pd 3d features of ~0.8 eV, consistent with results obtained for the bulk alloy. The experimentally measured CO desorption activation energies and vibrational frequencies do not correlate well with the surface sites expected from the bulk alloy composition but are more consistent with significant preferential segregation of gold to the alloy surface.

Keywords: X-ray photoelectron spectroscopy; Auger electron spectroscopy; CO; Temperature-programmed desorption; Au/Pd(1 1 1); Surface alloy

1. Introduction

Bimetallic surfaces exhibit a variety of interesting physical and chemical properties, which are quite different from those of the individual components [1,2]. One of the major goals of studying bimetallic surface-related phenomena is to better understand the unique function of mixed-metal alloys in heterogeneous catalysis. Several types of effects have been identified for bimetallic systems such as ligand effects, ensemble effects and strain effects [3–5].

In particular, palladium–gold bimetallic alloys have been found to provide both active and selective catalysts for a number of reactions including CO oxidation, cyclotrimerization of acetylene to benzene, vinyl acetate synthesis, selective oxidation of alcohols to aldehydes or ketones, oxidation of hydrogen to hydrogen peroxide, and hydrocarbon hydrogenation [6–15].

In addition, gold–palladium alloys provide rather ideal systems for fundamental study since gold and palladium are completely miscible in all proportions with only a slight lattice mismatch (~4.9%). Thus model gold–palladium catalysts can be made in ultrahigh vacuum by depositing a thin film of gold onto a Pd(1 1 1) single crystal and heating to various temperatures to allow the gold to diffuse into the palladium substrate. Merely adjusting the temperature and heating time allows alloys of various compositions to be obtained relatively straightforwardly. No ordered low-energy electron diffraction (LEED) structures other than the substrate (1 × 1) Bragg spots have been observed. In this case, the lattice spacing has been found to vary linearly with alloy composition both in the bulk [16] and on the surface [6]. This result implies that gold and palladium atoms may be rather randomly distributed on the surface, which allows the evolution of various surface ensembles to be calculated analytically, potentially providing a strategy for correlating the surface chemistry with the presence of various types of ensembles. The following explores the nature

* Corresponding author. Tel.: +1 414 229 5222; fax: +1 414 229 5036.
E-mail address: wtt@uwm.edu (W.T. Tysoe).

0039-6028/$ - see front matter © 2007 Elsevier B.V. All rights reserved.
doi:10.1016/j.susc.2007.02.028

of the alloys formed by depositing gold onto Pd(1 1 1) using electron spectroscopies and CO titration.

2. Experimental

The Pd(1 1 1) sample (1 cm diameter, 0.5 mm thick) was cleaned using a standard procedure, which consisted of cycles of argon ion bombardment (2 kV, 1 $\mu A/cm^2$) and annealing in 4×10^{-8} Torr of O_2 at 1000 K [17]. The cleanliness of the sample was judged using X-ray photoelectron spectroscopy (XPS) and oxygen titration where O_2 instead of CO desorbs following O_2 adsorption when the sample is carbon free. Gold was evaporated from a small alumina tube furnace [18]. In order to precisely control the temperature of gold, and therefore its evaporation rate, a C-type thermocouple was placed into the gold pellet. It has been found that controlled and reproducible evaporation rates can be achieved by maintaining a constant furnace temperature. Prior to evaporation, the gold source was extensively outgassed at 1300 K for several hours. During gold evaporation, the chamber pressure was maintained below 8×10^{-10} Torr.

X-ray photoelectron spectra (XPS) were collected in a UHV chamber operating at a base pressure of 2×10^{-10} Torr, which was equipped with Specs X-ray source and double-pass cylindrical mirror analyzer (CMA) [19]. Spectra were typically collected with a Mg Kα X-ray power of 250 W and at a pass energy of 50 eV. The binding energies were calibrated using the Pd $3d_{5/2}$ feature at 334.8 eV as a standard. The amount of gold deposited onto the surface was monitored using the intensities of Au $4f_{7/2}$ and Pd $3d_{3/2}$ features. Temperature-dependent XP spectra were collected by heating the sample to the indicated temperature for 5 min, then allowing the sample to cool to room temperature, following which the spectrum was recorded.

Temperature-programmed desorption (TPD) data were collected in an ultrahigh vacuum chamber operating at a base pressure of 8×10^{-11} Torr that has been described in detail elsewhere [20] where desorbing species were detected using a Dycor quadrupole mass spectrometer placed in line of sight of the sample. The sample could be cooled to 80 K by thermal contact to a liquid–nitrogen-filled reservoir and resistively heated to ~1200 K. Temperature-programmed desorption spectra were collected at a heating rate of 3.6 K/s. The temperature ramp and data collection were controlled using LabView software. This chamber was also equipped with a double-pass cylindrical mirror analyzer for Auger spectroscopy measurements and an ion-sputtering gun for sample cleaning. Auger electron spectra (AES) were collected using an electron beam energy of 3 keV and the amount of gold deposited onto the surface was monitored from the peak-to-peak intensities of Au_{NVV} and Pd_{MNN} Auger features. Temperature-dependent Auger data were collected in the same manner as XPS, where the sample was annealed to a certain temperatures for 5 min and cooled to room temperature before the data were collected.

Reflection adsorption infrared spectroscopy (RAIRS) data were collected using a Bruker Equinox infrared spectrometer equipped with a liquid-nitrogen-cooled, mercury–cadmium telluride detector. The complete light path was enclosed and purged with dry, CO_2-free air. Data were typically collected for 1000 scans at 4 cm^{-1} resolution.

3. Results

3.1. Au film deposition at 300 K

The Au film deposition rate, as well as the film thickness was calibrated using AES and XPS where, after depositing incremental amounts of Au onto Pd(1 1 1) at room temperature, the peak-to-peak intensities of Au_{NVV} and Pd_{MNN} Auger transitions and XPS signals in the Au $4f_{7/2}$ and Pd $3d_{3/2}$ regions were measured. A plot of the intensity ratios of the Au_{NVV} transition (at 71 eV kinetic energy) and the Pd_{MNN} feature (at 330 eV kinetic energy) is shown in Fig. 1(a) as a function of gold deposition time. These data are readily fit to multiple linear regions and each region corresponds to one monolayer of gold deposition. This reveals that identical times (~12 min at a gold source temperature of 1300 K) are required to deposit each monolayer (ML) of the gold film, indicating a layer-by-layer growth mode. As will be shown below, this is further verified by X-ray photoelectron spectroscopy.

Fig. 1(b) displays selected Auger spectra for 0, 3 and 7 ML of Au adsorbed onto Pd(1 1 1). This demonstrates that a 7 ML gold film completely blocks the Pd signal providing further evidence for layer-by-layer gold film growth. These spectra also emphasize that pure gold is deposited onto the Pd(1 1 1) substrate since no impurities, for example oxygen, sulfur or carbon are detected.

Fig. 2(a) displays the Au 4f XP spectra as a function of increasing gold deposition time on Pd(1 1 1) at room temperature where the Au 4f signal intensities increase with increasing gold deposition time. Note that weak signals are detected in this region prior to any gold deposition (Fig. 2(a), bottom spectrum) for two reasons: first, there is a weak Pd 4s feature at ~87 eV binding energy and second, a small amount of gold is evaporated from the source during initial outgassing. However, the Pd 4s signal is sufficiently weak that it does not significantly affect the subsequently measured Au 4f signal intensities. Fig. 2(b) displays the corresponding Pd 3d features. As expected, the Pd 3d signal intensity decreases with increasing gold deposition time. Note that the Pd $3d_{5/2}$ feature is almost exactly coincident with the Au $4d_{5/2}$ peak, so that only the Pd $3d_{3/2}$ signal was used to monitor the nature of the film. Fig. 2(c) plots the intensity of the Au $4f_{7/2}$ feature ratio to that of the Pd $3d_{3/2}$ peak as a function of gold deposition time. This displays identical behavior as that shown in Fig. 1(a), confirming that, following ~12 min of gold deposition, 1 ML of gold is formed. The binding energy of the

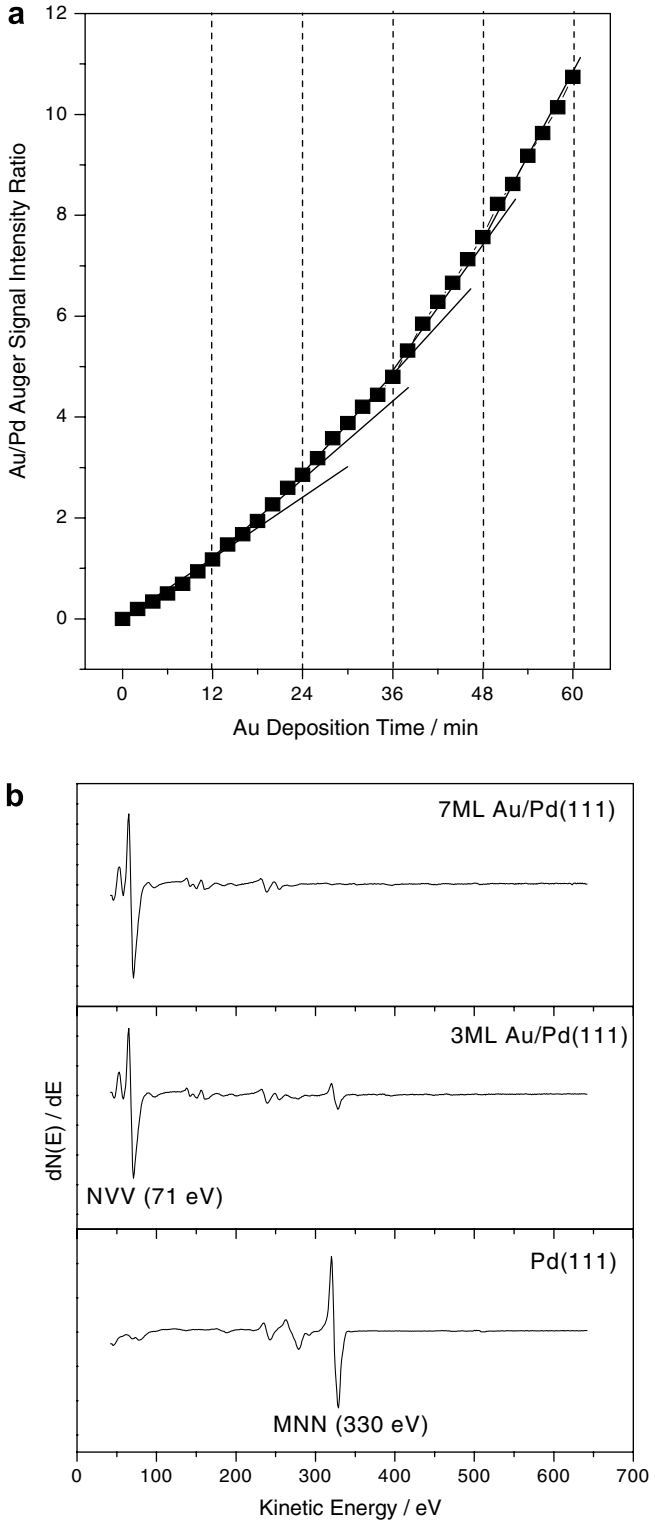

Fig. 1. (a) Plot of the intensity ratios of the Au_{NVV} transition (at 71 eV kinetic energy) and the Pd_{MNN} feature (at 330 eV kinetic energy) as a function of gold deposition time on a Pd(1 1 1) surface at 300 K. (b) Typical Auger spectra collected for the clean Pd(1 1 1) surface, and ones containing 3 and 7 monolayers (ML) of gold.

Au $4f_{7/2}$ peak is plotted as a function of coverage in Fig. 2(d) where the precision of the binding energy measurements is ±0.1 eV. The Au $4f_{7/2}$ BE is 83.1 ± 0.1 eV at a coverage of 0.15 ML, and shifts to 83.45 ± 0.1 eV at a 1 ML gold coverage, and increases further to 83.6 ± 0.1 eV (identical to that of pure gold [21]) at a coverage of 5 ML. The origin of this chemical shift will be discussed in more detail below.

3.2. Gold diffusion into Pd(1 1 1)

In order to investigate the diffusion of gold into the Pd(1 1 1) substrate and the resulting formation of alloys, a 7 ML thick gold film was first deposited at room temperature and then annealed to various temperatures for 5 min. After annealing at each temperature, X-ray photoelectron spectra were collected after cooling the sample to room temperature (~300 K).

Fig. 3 displays the XPS results after this procedure. Fig. 3(a) and (b) display the Au 4f and Pd 3d features, respectively. These data demonstrate that, as found previously [6], gold diffuses during annealing into the palladium substrate resulting in a decrease in the gold signal intensity and a concomitant increase in the palladium signal intensity with increasing temperature. Note that the gold signal intensity loss is due exclusively to diffusion into the bulk of the palladium since no gold is detected using temperature-programmed desorption. The integrated Au and Pd signal intensities and binding energies are plotted as a function of annealing temperature in Fig. 3(c) and (d), respectively. This reveals that that, when annealing the 7 ML Au/Pd(1 1 1) film from 300 to 500 K, no drastic changes occur in the Au and Pd signal intensities. Only after heating to 680 K and higher, are significant changes found (Fig. 3(c)). The binding energy of the Au $4f_{7/2}$ signal *decreases* from 83.6 ± 0.1 eV BE at 300 K to 83.1 ± 0.1 eV at 800 K and above (Fig. 3(d)), demonstrating the formation of a surface alloy on Pd(1 1 1) as found previously [22]. A corresponding increase is noted in the Pd $3d_{3/2}$ binding energy during annealing, shifting to a value close to pure palladium for the highest annealing temperature [23]. Similar annealing experiments have also been carried out for 2 and 4 ML Au/Pd(1 1 1) films (data not shown). Except for slight changes in the final gold binding energies following annealing, essentially identical relative gold and palladium signal intensities were found in each case.

Fig. 4(a) displays the ratio of Au 71 eV to Pd 330 eV Auger peak intensities for a film initially comprising 4 ML of Au on Pd(1 1 1), as a function of annealing temperature. It is clear that the gold film starts to intermix with the palladium substrate at about 500 K; extensive intermixing of Au and Pd is found at temperatures higher than 700 K, while after annealing the sample to 1110 K, almost no gold was detected. Shown also plotted on this figure are previous results for this experiment taken from reference [6] showing excellent agreement with the current data. Since gold and palladium intermix over the entire composition range [24], and since no gold desorption is detected in TPD, it is reasonable to assume that the vast majority of the gold

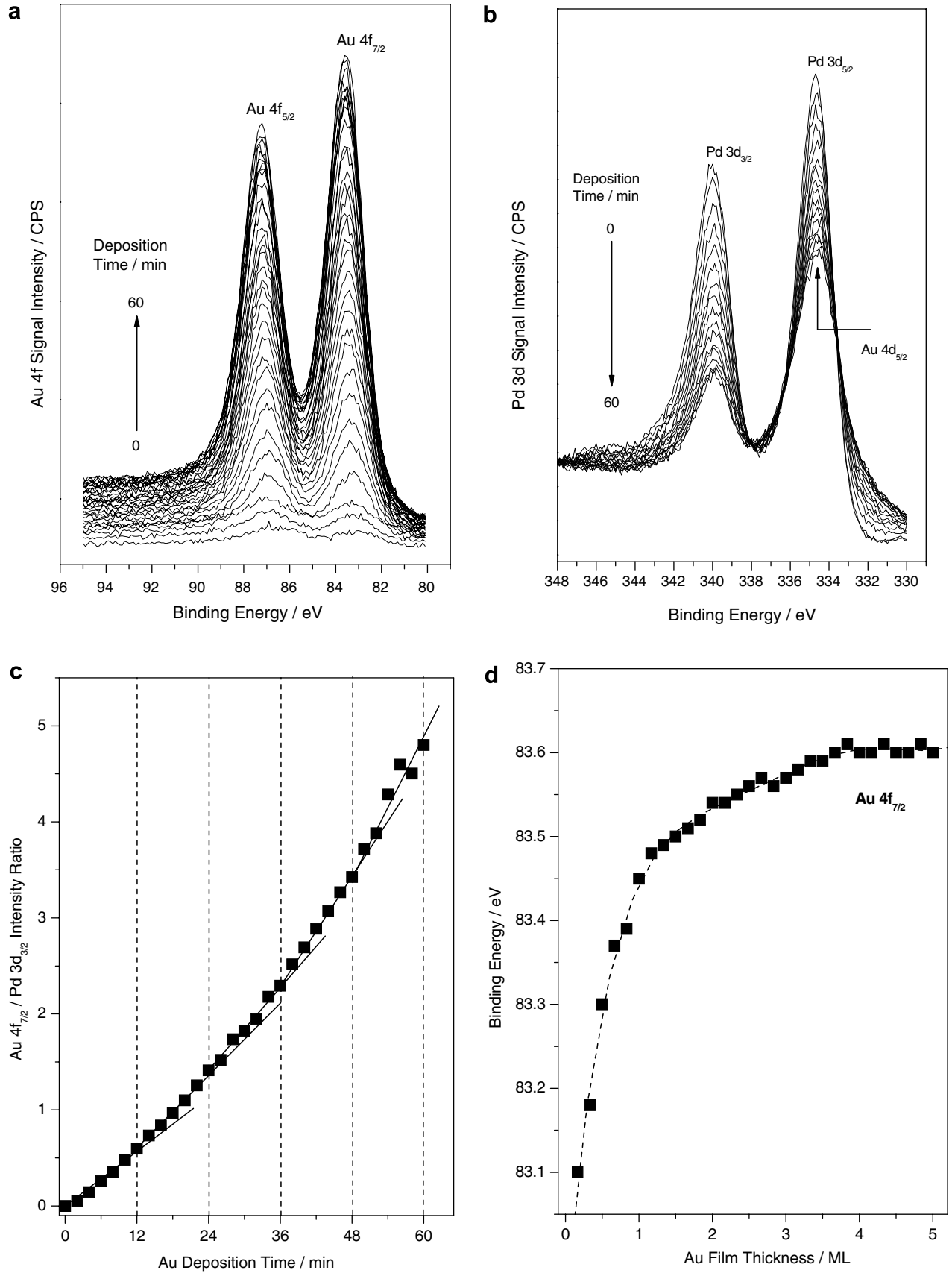

Fig. 2. (a) and (b) display the gold 4f and palladium 3d XPS regions as a function of deposition time for the evaporation of gold on a Pd(1 1 1) surface at 300 K. Graph (c) plots the intensity ratio of the Au $4f_{7/2}$ to the Pd $3d_{3/2}$ signals as a function of gold deposition time and graph (d) the corresponding position of the Au $4f_{7/2}$ feature as a function of deposition time.

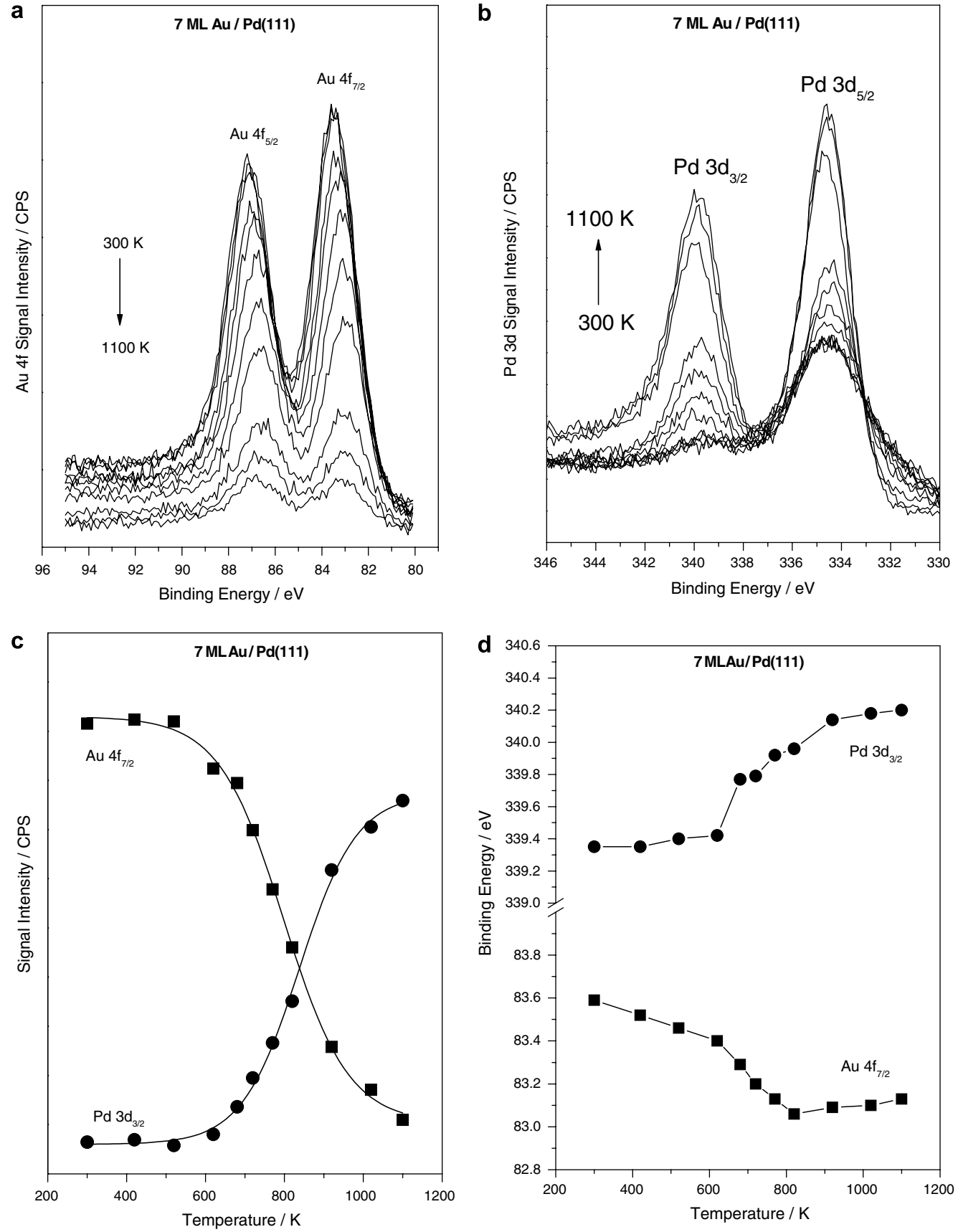

Fig. 3. (a) and (b) display the gold 4f and Pd 3d XPS regions as a function of annealing temperature following the deposition of 7 monolayers of gold on a Pd(1 1 1) surface at 300 K. Graph (c) plots the Au $4f_{7/2}$ and Pd $3d_{3/2}$ signals intensities and graph (d) their binding energies as a function of annealing temperature.

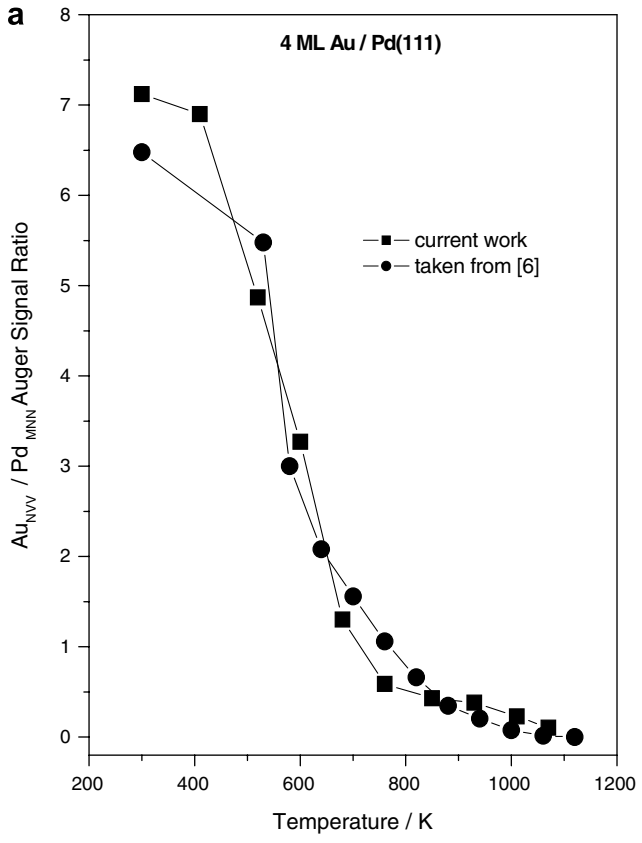

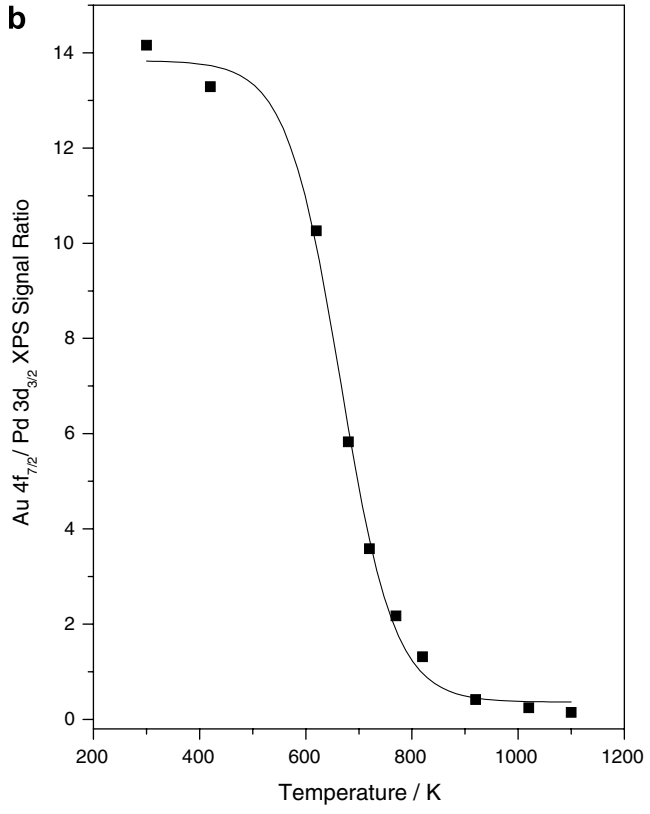

Fig. 4. (a) The ratio of the Au_{NVV} to the Pd_{MNN} Auger peak-to-peak intensities and (b) the ratio of the Au $4f_{7/2}$ and Pd $3d_{3/2}$ XPS signals as a function of annealing temperature.

film diffuses into the palladium substrate. A similar plot of the gold to palladium ratio taken from the XPS data of Fig. 3(c) is displayed in Fig. 4(b). The shape of this curve is essentially identical to that displayed in Fig. 4(a) expect that the gold signals are slightly higher reflecting the larger initial gold coverage.

3.3. Depth profile of gold films in Pd(111)

In order to understand in greater detail the diffusion of Au into the Pd substrate, Ar^+ (3000 eV, 1.5 μA) bombardment was employed on 7 ML Au/Pd(111) annealed to 1100 K. After various bombardment intervals, XP spectra were collected. Fig. 5 shows the intensities of Au $4f_{7/2}$ and Pd $3d_{3/2}$ photoemission peaks as a function of sputtering time. Shown as a horizontal line is the Pd $3d_{3/2}$ signal measured for pure palladium. The intensity of Au $4f_{7/2}$ signal decreases with increasing sputtering time while the intensity of Pd $3d_{3/2}$ peak increases. A rapid decrease in the gold signal intensity was found during the first 5 min of bombardment. The concentration varies much more slowly for longer bombardment times suggesting that gold tends to segregate to the surface. However, even after 240 min of sputtering, only ~60% Au was removed from sample. It requires more than 20 h of bombarding to remove all the deposited gold from the substrate.

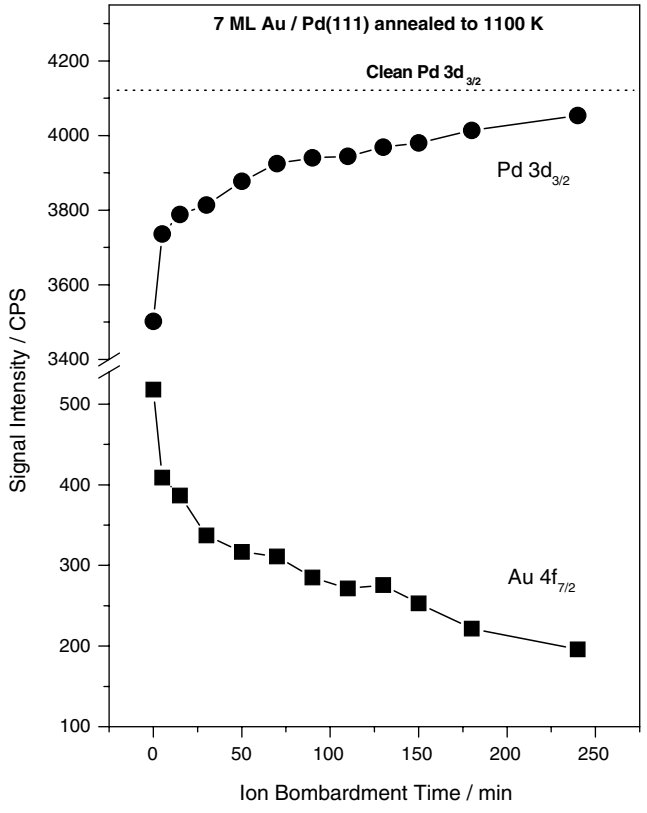

Fig. 5. Argon ion (3000 eV, 1.5 μA) bombardment depth profile for 7 ML film of gold on Pd(111) annealed to 1100 K monitoring the Au $4f_{7/2}$ and Pd $3d_{3/2}$ XPS signals as a function of bombardment time.

3.4. CO adsorption on Au/Pd alloys: TPD and RAIRS

In order to gain more information about the composition of the outermost layer of the Au/Pd(1 1 1) alloy, TPD experiments were carried out for CO on Au/Pd(1 1 1). Extensive work has been carried out previously to study CO/Pd(1 1 1) using LEED, TPD and RAIRS and demonstrates that, up to a coverage of 0.33, CO preferentially adsorbs on 3-fold hollow sites, and then on bridge sites at a coverage of 0.5. At higher coverages, both atop and bridge sites are occupied [25, and references therein]. Fig. 6 shows a sequence of CO TPD results for a 4 ML film of Au/Pd(1 1 1) after annealing to successively higher temperatures. The spectra are in good agreement with those reported previously for CO on Au/Pd(1 1 1) alloys [6]. For these TPD experiments, 10 L CO was adsorbed at 80 K to saturate the surface. At low annealing temperatures (<620 K), a single desorption peak occurs at 120 K, due to CO desorption from gold atop sites [10]. When annealing the sample to 620 K, an additional small CO desorption peak appears at 298 K. This desorption state saturates when the sample has been annealed to 800 K and above, accompanied by a desorption temperature increase to 334 K. A third desorption state appears at

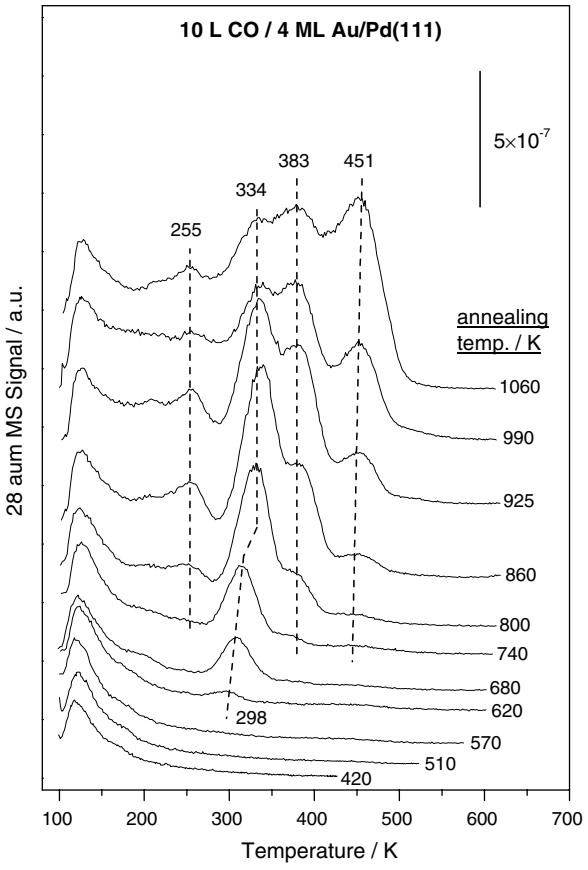

Fig. 6. Temperature-programmed desorption spectra (28 amu, CO) collected using a heating rate of 3.6 K/s for a 4 ML film of Au/Pd(1 1 1) after annealing successively to higher temperatures where the annealing temperatures are marked adjacent to the corresponding spectrum.

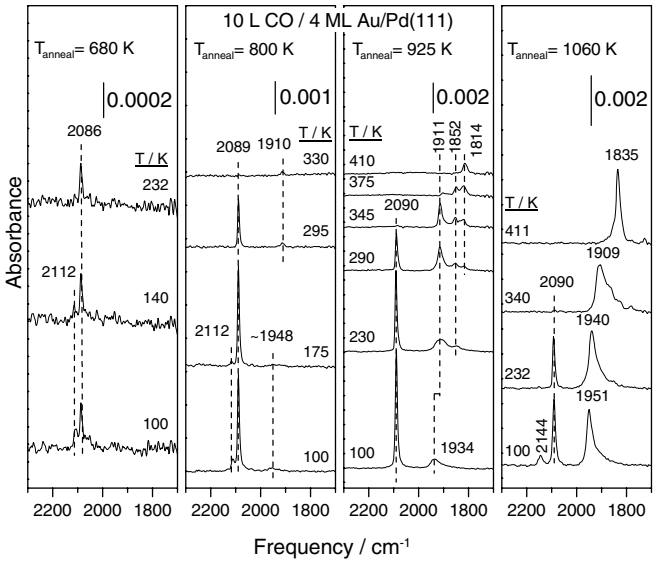

Fig. 7. RAIRS spectra following 4 ML Au adsorption on Pd(1 1 1) and after annealing to higher temperatures, where 10 L of CO is allowed to adsorb on the surface after each annealing step.

~383 K after annealing the sample to 740 K. Two more states occur at ~250 and ~430 K after further annealing the sample to 800 K.

Fig. 7 displays the corresponding RAIRS results following 4 ML Au adsorption on Pd(1 1 1) and after annealing to higher temperatures, where 10 L of CO is allowed to adsorb on the surface after each annealing step. The as-formed Au/Pd(1 1 1) film at room temperature only displays one CO stretching feature at 2112 cm^{-1} (data not shown), which is assigned to CO adsorption onto Au atop sites. When the surface is annealed to 680 K, in addition to this feature, another CO stretching mode appears at 2086 cm^{-1} (left panel), assigned to CO adsorption onto Au atop sites. It should be noted that following this annealing temperature, the alloy is predominantly composed of gold (~80%, Fig. 4). However, CO appears to preferentially adsorb on Pd sites. The 2112 cm^{-1} feature disappears on warming the sample to 232 K while the 2086 cm^{-1} feature disappears at 300 K (data not shown). When the sample is annealed to 800 K (second panel), the relative intensity ratios of these two features change substantially so that the 2089 cm^{-1} feature become much more intense than the 2112 cm^{-1} peak. A weak and broad feature appears at ~1948 cm^{-1} at 100 and 175 K, and shifts to 1910 cm^{-1} on heating to 295 and 330 K. After annealing the alloy to 925 K (third panel), the 2112 cm^{-1} signal becomes undetectable, even though some gold still remains on the surface (Figs. 3 and 4). The 2090 cm^{-1} feature disappears when the sample is warmed to 345 K and the 1911 cm^{-1} feature intensifies compared with the sample formed at an annealing temperature of 800 K, and two more features appear at 1852 and 1814 cm^{-1} on heating the alloy to 290 K. The 1852 cm^{-1} feature disappears at on warming to 411 K and the 1814 cm^{-1} feature remains

until 450 K. On annealing the alloy to 1060 K (right hand panel), besides the 2090 cm^{-1} feature, a curious 2144 cm^{-1} signal is detected at 100 K. Below 2000 cm^{-1}, broad features appear and these shift to lower frequencies on heating.

4. Discussion

The growth mode of one metal on another is affected by a number of factors such as surface free energies, growth rate, substrate temperature and strain energies. From a thermo-chemical point of view, three different growth modes are expected: layer-by-layer or Frank–van der Merwe (FV) growth, layer-plus-island or Stranski–Krastanov (SK) growth mode, and island or Volmer–Weber (VW) growth [26]. Generally the surface free energies of the two pure metals and the interface play more important roles than other factors. However, while the interfacial free energy is usually not available, the surface free energy of palladium is 2.05 J/m^2 [27], and that of gold is 1.63 J/m^2 [28] and there is only ~4.9% lattice mismatch between Au(1 1 1) and Pd(1 1 1) surfaces [24] so that the strain energy is not likely to be a crucial factor in determining the growth mode. It is therefore reasonable to assume predominantly layer-by-layer growth of gold on the Pd(1 1 1) surface. Our results (Figs. 1 and 2) confirm that it is indeed the case and that it requires ~12 min to form each monolayer of gold on Pd(1 1 1) using the sample temperature and geometry of our gold evaporation source. This growth mode is consistent with the work of Silverman [29] and Thiel and Mitchell who also found layer-by-layer growth of gold on Pd(1 1 0) [30,31].

Unlike the reverse Pd/Au(1 1 1) system, where annealing always forms an ordered $(\sqrt{3}\times\sqrt{3})R30°$ surface alloy [32], the Au/Pd(1 1 1) system shows no ordered LEED patterns except for the substrate (1×1) Bragg spots that are also observed during annealing [6]. The inter-diffusion of gold into palladium is negligible at room temperature and becomes faster when the sample is annealed to 680 K. The intermixing of Au with Pd can cause electronic perturbations of the two metals. Core level spectroscopic characterization of palladium and gold may therefore provide insights into charge transfer/rehybridization that occurs in this system. The Au $4f_{7/2}$ and Pd $3d_{3/2}$ binding energies are ~83.6 eV and ~339.4 eV, respectively at room temperature for 7 ML Au/Pd(1 1 1) (Fig. 3(d)). The Au $4f_{7/2}$ BE decreases to ~83.4 eV when annealing the sample to 620 K and a dramatic binding energy change is found while further annealing to 800 K, where the Au $4f_{7/2}$ BE becomes ~83.1 eV. The Pd $3d_{3/2}$ BE increases to ~340.1 eV when annealing the sample to 1080 K, which is identical to clean Pd [23]. These data clearly demonstrate alloy formation during annealing. Some previous XPS work has been carried out on bulk alloys. A chemical shift of −0.2 eV was found in the Au $4f_{7/2}$ feature for a $Au_{45}Pd_{55}$ alloy [33]. The Auger data of Fig. 4 suggest that an alloy of this composition should be formed by annealing to ~600 K, and a similar chemical shift is found experimentally for a thin alloy film formed on Pd(1 1 1) (Fig. 3(d)). Similarly, Hufner et al. found a −0.7 eV chemical shift for the Au $4f_{7/2}$ feature of a $Au_{10}Pd_{90}$ alloy [34]. Again, the data of Fig. 4 indicate that an alloy of this composition is formed by annealing to ~800 K, and the chemical shift measured in this work is -0.55 ± 0.1 eV. This suggests that the Auger calibration shown in Fig. 4 from this and previous work [6] yields reasonably accurate alloy compositions. Thus, the chemical shifts displayed in Fig. 3(d) are consistent with the behavior found for the bulk alloy. As has been suggested previously, one has to be very cautious in judging the net electron transfer during bimetallic alloying using photoelectron spectroscopy because of the rather complicated combination of initial and final state effects [35]. Nevertheless, the Pauling electronegativities of palladium (2.20) and gold (2.54) suggest that there should be a slight electron transfer from palladium to the gold, consistent with the observed chemical shifts. It is worth commenting on the Au $4f_{7/2}$ binding energy increase during gold deposition at room temperature shown in Fig. 2(d). Apparently alloy formation occurs after annealing to 500 K and above so that a BE increase in this case is unlikely due to alloy formation. As the submonolayer gold grows two-dimensionally as expected for a layer-by-layer growth mechanism, the binding energy increase may reflect a coordination or adsorption site dependence [36]. This is corroborated by the fact that the binding energy increases rapidly and almost linearly within the monolayer range but becomes much slower at higher coverages.

Pd/Au surface alloys can also be generated using other strategies. Goodman and co-workers [22] co-deposited 5 ML of Au and 5 ML of Pd onto Mo(1 1 0) followed by annealing to different temperatures. They found a stable surface alloy formed between 700 and 1000 K, which has a surface composition of 80% Au and 20% Pd [22] suggesting that the surface is enriched in gold compared to the bulk, consistent with gold's lower surface energy and the data shown in Fig. 5. Koel and co-workers also found the formation of a Pd/Au surface alloy by annealing a Pd/Au(1 1 1) sample to higher temperatures [21].

The techniques applied in the current study for surface composition determination, namely AES and XPS are surface sensitive but provide information not restricted to the topmost 1–2 layers. However, the data shown in Fig. 5 indicate that gold can diffuse rather deeply into the palladium substrate since complete removal of deposited gold requires extensive ion bombardment. This means that AES and XPS, since these have detection depths greater than a monolayer, underestimate the real Au/Pd atomic ratio at the topmost layer.

The surface composition was characterized by CO adsorption using a combination of TPD and RAIRS. The CO desorption peak at ~120 K (Fig. 6), as well as the 2112 cm^{-1} RAIRS feature (Fig. 7) is assigned to CO adsorption on gold atop sites. Goodman and coworkers also found a similar low-temperature desorption peak at

Table 1
Vibrational frequencies and heats of adsorption of carbon monoxide adsorbed on various sites of a Au/Pd(111) alloy

	Vibrational frequency/cm^{-1}	Desorption activation energy/kJ/mol
Au atop site	2112	30
Pd atop site	2086–2089	76–86
Pd bridge site	1911–1934	99
Pd 3-fold hollow	<1900	117
Au atop modified by Pd	2144	65

125 K for the Au/Pd/Mo(110) system [10], also assigned to atop CO on Au. With increasing annealing temperature, a second desorption peak appears at 298 K (Fig. 6). This peak shifts to a higher temperature and the peak intensity increases with increasing surface palladium composition. Based on work by Guo and Yates [23], this is assigned to CO on atop palladium sites. This correlates with the 2086–2090 cm^{-1} infrared feature (Fig. 7). Upon further annealing, several more CO desorption states appear: the peak at 383 K is assigned to desorption from bridge sites and that at 451 K to desorption from 3-fold hollow sites (Fig. 6). It is a little more difficult to make precise RAIRS assignments because several CO features coexist below 2000 cm^{-1}, especially after the sample has been annealed to 925 K. However, it is reasonable to assign the features between 2000 and 1900 cm^{-1} to CO adsorption on bridge sites and features below 1900 cm^{-1} to CO adsorption on 3-fold hollow sites [37]. Desorption at 255 K (Fig. 6) is tentatively assigned to CO adsorption on gold atop sites that are modified by Pd atoms or Pd–Au bridge sites. These results are consistent with previous work by Lambert and coworkers [6]. These assignments are summarized in Table 1, which displays the vibrational frequencies and desorption activation energies calculated using the Redhead equation [38] assuming a desorption pre-exponential factor of 1×10^{13} s^{-1}, for various sites on the Au/Pd alloy.

It is, in principle, possible to correlate the CO site occupancies with the surface composition of the gold–palladium alloys assuming that the gold and palladium atoms are randomly distributed on the surface. In practice, this is complicated by the fact that different sites are occupied at different sample temperatures (see Fig. 7), in particular when the palladium coverage becomes higher. At low palladium coverages, and thus low annealing temperatures up to ~800 K, only atop palladium and gold sites appear to be occupied. In this case, the number of isolated palladium sites is simply proportional to $\Theta(\mathrm{Pd})(1-\Theta(\mathrm{Pd}))^6$. As the coverage increase, isolated bridge sites will appear, being proportional to the probability that two palladium atoms will occupy neighboring sites and that the surrounding sites are gold, and is given by $3\Theta(\mathrm{Pd})^2(1-\Theta(\mathrm{Pd}))^8$. The maximum number of isolated palladium sites will thus appear at $\Theta(\mathrm{Pd}) \sim 0.2$; at higher coverages, dimers and larger clusters start to appear. According to the data of Fig. 4, this will occur when the gold film on palladium has been heated to ~520 K while Fig. 6 shows no CO desorption from atop palladium sites. According to both infrared (Fig. 7) and TPD (Fig. 6), a small amount of CO desorption is found only when the sample has been annealed to 620 K and significant signal is found only at ~680 K. The data of Fig. 4 indicate that these annealing temperatures produce palladium concentrations in the near-surface region of ~0.6 and 0.8, respectively. There are a number of possible origins for this large discrepancy. It may be that isolated palladium atoms are strongly electronically modified by the surrounding gold atoms such that they are no longer capable of strongly binding carbon monoxide. Supports for this notion comes from the observation that isolated gold atoms adsorb CO much more strongly than bulk gold (see Table 1). An alternative possibility is that both Auger (Fig. 4) and XPS (Fig. 3) are probing sufficiently far into the sample that they are primarily measuring the alloy composition in the near-surface region and that the gold coverage at the surface is higher than that due to the lower gold surface energy. The depth profile data of Fig. 5 indicates that this is the case and such surface enrichment by gold has been observed previously by Goodman et al. for Au–Pd alloys grown on a Mo(110) substrate by measuring the surface composition of a series of alloy films using low-energy ion surface scattering (LEISS) [22]. In order to analyze these data, the bulk palladium and gold concentrations are designated C_{Pd} and C_{Au}, respectively, and the corresponding surface gold and palladium coverages as Θ_{Pd} and Θ_{Au} and, assuming that the bulk and surface are in equilibrium, gives:

$$\frac{\Theta_{\mathrm{Pd}}}{C_{\mathrm{Pd}}} = K_{\mathrm{Pd}} \quad \text{and} \quad \frac{\Theta_{\mathrm{Au}}}{C_{\mathrm{Au}}} = K_{\mathrm{Au}}. \tag{1}$$

Writing the mole fraction of the alloy that comprises gold X_{Au} as $X_{\mathrm{Au}} = \frac{C_{\mathrm{Au}}}{C_{\mathrm{Pd}}+C_{\mathrm{Au}}}$ and normalizing the gold and palladium coverages to unity so that: $\Theta_{\mathrm{Pd}} + \Theta_{\mathrm{Au}} = 1$, then:

$$\Theta_{\mathrm{Au}} = \frac{KX_{\mathrm{Au}}}{1-(1-K)X_{\mathrm{Au}}}, \tag{2}$$

where $K = K_{\mathrm{Au}}/K_{\mathrm{Pd}}$. As noted above, Goodman et al. have used LEISS to measure the surface composition of various alloys of gold and palladium formed on a Mo(110) substrate by heating to 800 K for 20 min [22]. Equation (2) fits extremely well to their experimental data yielding a value of $K = 5.5 \pm 0.1$. The surface structure of bulk $Pd_{40}Au_{60}$ and $Pd_{60}Au_{40}$ alloys have also been measured using LEISS and also found surface gold segregation with gold coverages of ~0.85 and 0.7, respectively for those alloys. Using equation (2) with the value of K measured from Goodman's data predicts coverages of ~0.89 and 0.78, respectively for the two alloys. These values are in reasonable agreement with the experimental data further validating equation (2). It should be noted that the ratio of equilibrium constants K will be temperature dependent and that the experiments in this work were carried out by annealing to high temperatures and cooling to 300 K to perform the surface analyses. It is thus likely that the extent of gold segregation to the surface is some metastable state frozen in as

the sample is cooled. Nevertheless, equation (2) appears to provide a reasonable measure of the extent of gold surface segregation on Au–Pd alloys. Thus, combining the alloy compositions in the near-surface region measured from the data in Fig. 4 with estimates of the extent of surface segregation from equation (2) now allows the nature of the surface sites to be correlated with the surface composition.

This strategy suggests that the surface gold coverages in the infrared data shown in Fig. 7 are ~0.81, 0.43 and 0.15 monolayers for samples that have been annealed to 680, 800 and 925 K, respectively. RAIRS data have been collected previously for a 5 ML Pd/5 ML Au/Mo(1 1 0) film annealed to 800 K for 20 min to yield a surface gold coverage of ~0.82 [22]. From the above discussion, this should yield a surface composition almost identical to that found by annealing to 680 K (Fig. 7). Indeed, RAIRS spectra for CO on each surface yielded peaks at 2086 (2087 cm^{-1} in reference [22]) and 2112 cm^{-1} [22]. In addition, the variations in intensity on warming are essentially identical in each case. This result provides preliminary confirmation that the CO titration data can be analyzed by assuming that the surface is enriched with gold compared to the bulk and that the segregation is reasonably well described by equation (2) with a value of $K \sim 5.5$.

The CO desorption yield, measured from the data in Fig. 6, is plotted for the various desorption states *versus* the surface palladium coverage calculated as described above for desorption from atop (■), bridge (●) and 3-fold (▲) sites (see Table 1) as well as the total normalized CO desorption yield (▼) in Fig. 8. The thick solid line plots the calculated number of isolated palladium atoms as a function of palladium coverage assuming that the gold and palladium are randomly distributed on the surface. As noted above, the palladium coverage calibration assumes that the XPS signal intensities reasonably reflect the alloy composition in the near-surface region and that the preferential segregation of gold is well described by equation (2).

At the lowest palladium coverages (Θ(Pd) < ~0.2), the data points are in good agreement with the calculated number of isolated (atop) palladium sites (thick solid line). However, as the palladium coverage exceeds ~1/3, the coverage of CO adsorbed on atop sites increases more rapidly with palladium coverage. Even at palladium coverages above 0.5, both TPD (Figs. 6 and 8) and RAIRS (Fig. 7) indicate that CO still adsorbs preferentially on atop sites. It is only for palladium coverages above ~0.7 that bridge and 3-fold sites become occupied. The most straightforward explanation for this phenomenon is that palladium atoms remain isolated from each other and are not randomly distributed on the surface. This conclusion, however, does not agree with the observed lack of LEED patterns for the Au/Pd(1 1 1) alloy and may be due to an electronic modification of small clusters (i.e., dimers and trimers) by the surrounding gold that causes preferential adsorption on atop sites even when other sites are available. A final resolution of this issue will come from more detailed structural measurements, in particular LEISS to unequivocally determine the structure of the outermost surface and STM to establish exactly how randomly these are distributed.

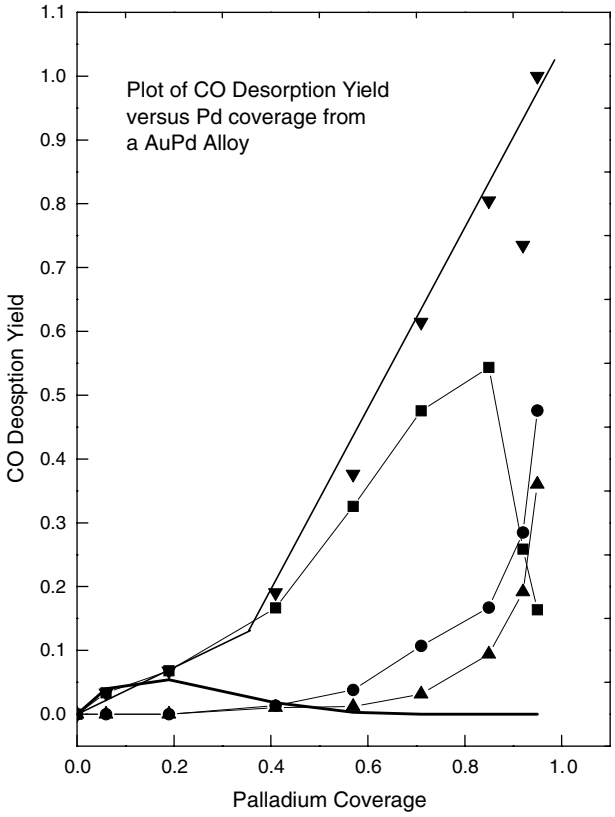

Fig. 8. Plot of the CO desorption yields as a function of palladium coverage taken from the data of Fig. 6 for desorption from atop (■), bridge (●) and three-fold (▲) sites as well as total relative CO desorption yield (▼). The thick solid line plots the calculated number of isolated palladium atoms as a function of palladium coverage assuming that the gold and palladium are randomly distributed on the surface.

5. Conclusions

Au is deposited on a Pd(1 1 1) substrate and the resulting film is investigated using AES, XPS and CO titration. It is found that Au film grows layer-by-layer (Frank–van der Merwe model) on Pd (1 1 1). Au and Pd intermix quickly at 600 K and above where XPS demonstrates alloy formation. Various surface adsorption sites are readily determined using CO titration. This work demonstrates that by adsorbing various amount of Au on Pd(1 1 1) and annealing to various temperatures, a full range of surface Au/Pd compositions can be achieved.

Acknowledgement

We gratefully acknowledge the support of this work by the US Department of Energy, Office of Basic Energy Sciences, Division of Chemical science, under Grant no. DE-FG02-92ER14289.

References

[1] J. Rodriguez, Surf. Sci. Rep. 24 (1996) 223.
[2] D.P. Woodruff, The Chemical Physics of Solid Surfaces Alloy Surfaces and Surface Alloys, Elsevier, Amsterdam, 2002, vol. 10.
[3] M. Fernandez-Garcia, J.A. Anderson, G.L. Haller, J. Phys. Chem. 100 (1996) 16247.
[4] V. Ponec, Appl. Catal. A 222 (2001) 31.
[5] T. Hager, H. Rauscher, R.J. Behm, Surf. Sci. 558 (2004) 181.
[6] C.J. Baddeley, M. Tikhov, C. Hardacre, J.R. Lomas, R.M. Lambert, J. Phys. Chem. 100 (1996) 2189.
[7] C.J. Baddeley, R.M. Ormerod, A.W. Stephenson, R.M. Lambert, J. Phys. Chem. 99 (1995) 5146.
[8] Y.F. Han, D. Kumar, D.W. Goodman, J. Catal. 230 (2005) 353.
[9] A.M. Venezia, V. La Parola, B. Pawelec, J.L.G. Fierro, Appl. Catal. A 264 (2004) 43.
[10] M.S. Chen, D. Kumar, C.W. Yi, D.W. Goodman, Science 310 (2005) 291.
[11] L. Piccolo, A. Piednoir, J.-C. Bertolini, Surf. Sci. 592 (2005) 169.
[12] N. Dimitratos, A. Villa, D. Wang, F. Porta, D. Su, L. Prati, J. Catal. 244 (2006) 113.
[13] D.I. Enache, J.K. Edwards, P. Landon, B. Solsona-Espriu, A.F. Carley, et al., Science 311 (2006) 362.
[14] P. Landon, P.J. Collier, A.J. Papworth, C.J. Kiely, G.J. Hutchings, Chem. Commun. 18 (2002) 2058.
[15] J.K. Edwards, B.E. Solsona, P. Landon, A.F. Carley, et al., J. Catal. 236 (2005) 69.
[16] J. Banhart, Phys. Rev. B 53 (1996) 7128.
[17] D. Stacchiola, L. Burkholder, W.T. Tysoe, Surf. Sci. 511 (2002) 215.
[18] W.J. Wytenburg, R.M. Lambert, J. Vac. Sci. Technol. A 10 (1992) 3597.
[19] Yilin Wang, Feng Gao, W.T. Tysoe, J. Mol Catal A-Chem. 236 (2005) 18.
[20] M. Kaltchev, A.W. Thompson, W.T. Tysoe, Surf. Sci. 391 (1997) 14.
[21] B.E. Koel, A. Sellidj, M.T. Paffett, Phys. Rev. B 46 (1992) 7846.
[22] C.W. Yi, K. Luo, T. Wei, D.W. Goodman, J. Phys. Chem. B 109 (2005) 18535.
[23] C.D. Wagner, W.M. Riggs, L.E. Davis, J.F. Moulder, G.E. Muilenberg, Handbook of X-ray Photoelectron Spectroscopy, Perkin-Elmer Co., Minnesota, 1979.
[24] D.L. Weissman-Wenocur, P.M. Stefan, B.B. Pate, M.L. Shek, I. Lindau, W.E. Spicer, Phys. Rev. B 27 (1983) 3308.
[25] X. Guo, J.T. Yates Jr., J. Chem. Phys. 90 (1989) 6761.
[26] A. Zangwill, Physics at Surfaces, Cambridge University Press, Cambridge, 1988.
[27] L.Z. Mezey, J. Giber, Jpn. J. Appt. Phys. 11 (1982) 1569.
[28] W.R. Tyson, W.A. Miller, Surf. Sci. 62 (1977) 267.
[29] Y. Kuk, L.C. Feldman, P.J. Silverman, Phys. Rev. Lett. 50 (1983) 511.
[30] P.J. Schmitz, H.C. Kang, W.-Y. Leung, P.A. Thiel, Surf. Sci. 248 (1991) 287.
[31] M. Vos, I.V. Mitchell, Phys. Rev. B 45 (1992) 9398.
[32] C.J. Baddeley, C.J. Barnes, A. Wander, R.M. Ormerod, D.A. King, R.M. Lambert, Surf. Sci. 314 (1994) 1.
[33] J. Hedman, M. Klasson, R. Nilsson, C. Nordling, M.F. Sorokina, O.I. Kljushnikov, S.A. Nemnonov, V.A. Trapeznikov, V.G. Zyranov, Phys. Scripta 4 (1971) 195.
[34] S. Hufner, G.K. Wertheim, J.H. Wernick, Solid State Commun. 17 (1975) 417.
[35] W.F. Egelhoff Jr., Surf. Sci. Rep. 6 (1987) 253.
[36] P.H. Citrin, G.K. Wertheim, Y. Baer, Phys. Rev. Lett. 41 (1978) 1425.
[37] F.M. Hoffmann, Surf. Sci. Rep. 3 (1983) 107.
[38] P.A. Redhead, Vacuum 12 (1962) 203.